Supporting Information

Divergent A-Site Regulation Mechanisms in Rare-Earth and Alkaline-Earth Nickelates for Unlocking Bifunctional Oxygen Electrocatalysis

Taoda Liu[1,2], Yuhang Dou[1], Tian Ouyang[2], Sheng Ma[2], Zongqing Tian[1], Zhiwei Peng[1,3], Xiaoling He[2], Wenyan Tao[2]*, Yinghua Niu[1]*, Weiqiang Lv[1,3]*

1 School of Physics & School of Integrated Circuit Science and Engineering (Exemplary School of Microelectronics), University of Electronic Science and Technology of China, Chengdu 611731, P. R. China

2 School of Materials and New Energy, South China Normal University, Shanwei, 510006, P. R. China

3 Yangtze River Delta Research Institute (Huzhou), University of Electronic Science and Technology of China, Huzhou 313000, P. R. China

*Corresponding authors:

Wenyan Tao: E-mail: taowenyan@m.scnu.edu.cn

Yinghua Niu: E-mail:yh_niu@uestc.edu.cn

Weiqiang Lv: E-mail:eselwq@uestc.edu.cn

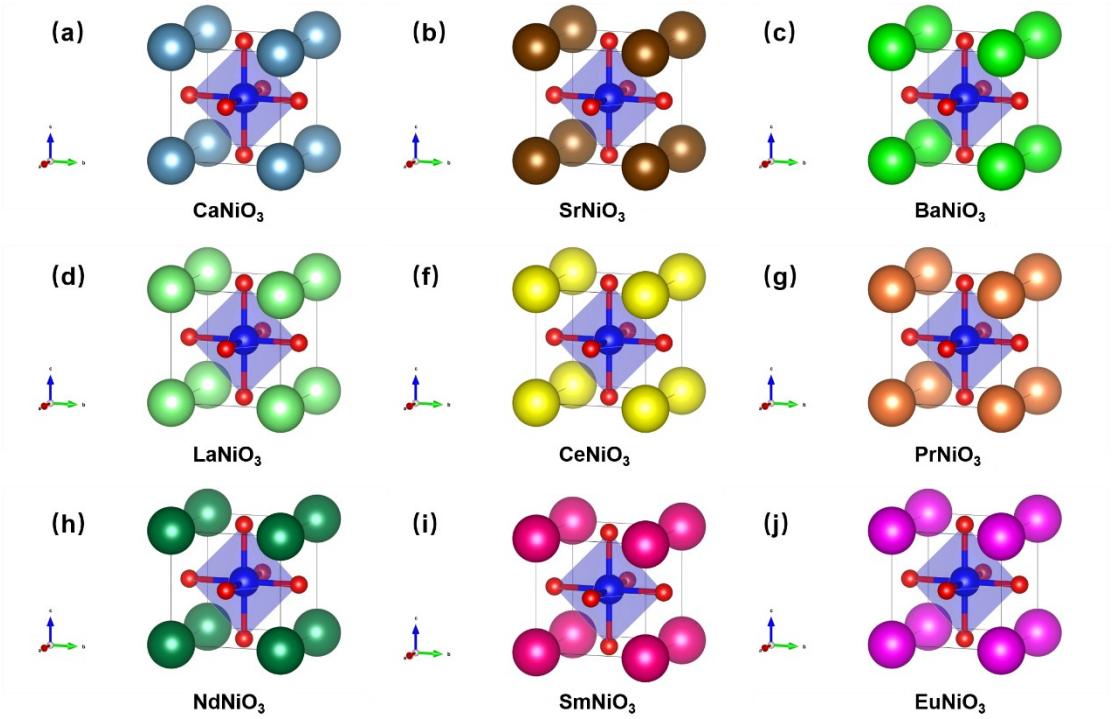

Figure S1. Bulk structure of $ANiO_3$ perovskites: (a)$CaNiO_3$, (b)$SrNiO_3$, (c)$BaNiO_3$, (d)$LaNiO_3$, (e)$CeNiO_3$, (f) $PrNiO_3$, (g) $NdNiO_3$, (h)$SmNiO_3$, (i)$EuNiO_3$,. Ca, Sr, Ba, La, Ce, Pr, Nd, Sm, Eu,Ni, and O atoms arepresented as light blue, brown, green, light green, yellow, orange, dark green, pink, purple, blue and red, respectively

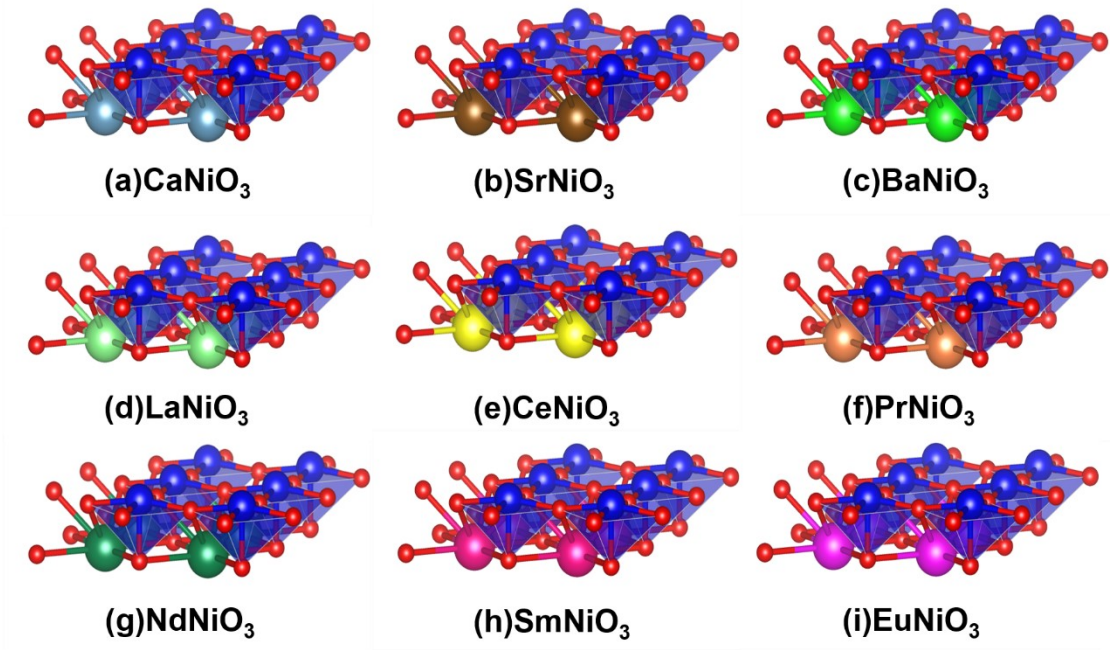

Figure S2. Optimization of surface structure of barium based perovskite (001) Ni-O: (a)$CaNiO_3$, (b)$SrNiO_3$, (c)$BaNiO_3$, (d)$LaNiO_3$, (e)$CeNiO_3$, (f) $PrNiO_3$, (g) $NdNiO_3$, (h)$SmNiO_3$, (i)$EuNiO_3$,. Ca, Sr, Ba, La, Ce, Pr, Nd, Sm, Eu, Ni, and O atoms

arepresented as light blue, brown, green, light green, yellow, orange, dark green, pink, purple, blue and red, respectively

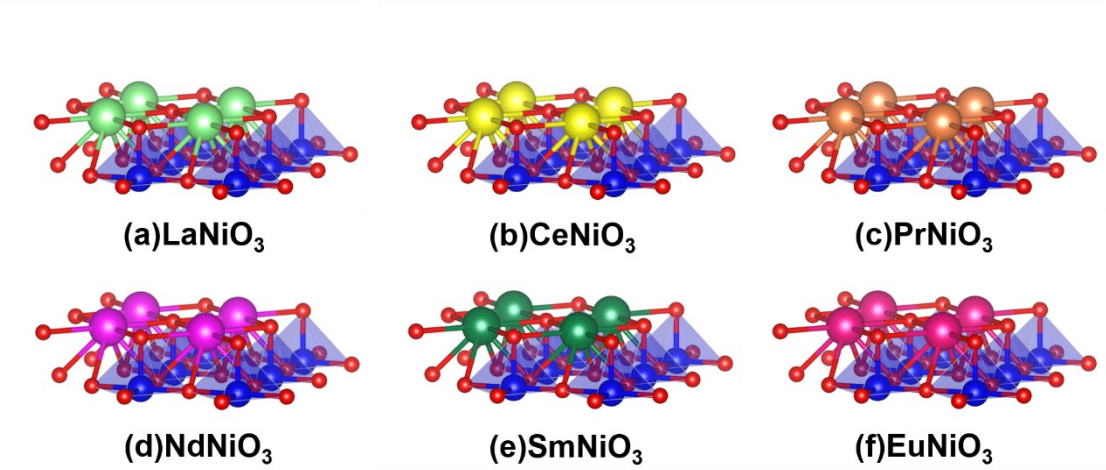

Figure S3. Optimization of surface structure of barium based perovskite (001) AO: (a)$LaNiO_3$, (b)$CeNiO_3$, (c) $PrNiO_3$, (d) $NdNiO_3$, (e)$SmNiO_3$, (f)$EuNiO_3$,. La, Ce, Pr, Nd, Sm, Eu, Ni, and O atoms arepresented as light green, yellow, orange, dark green, pink, purple, blue and red, respectively

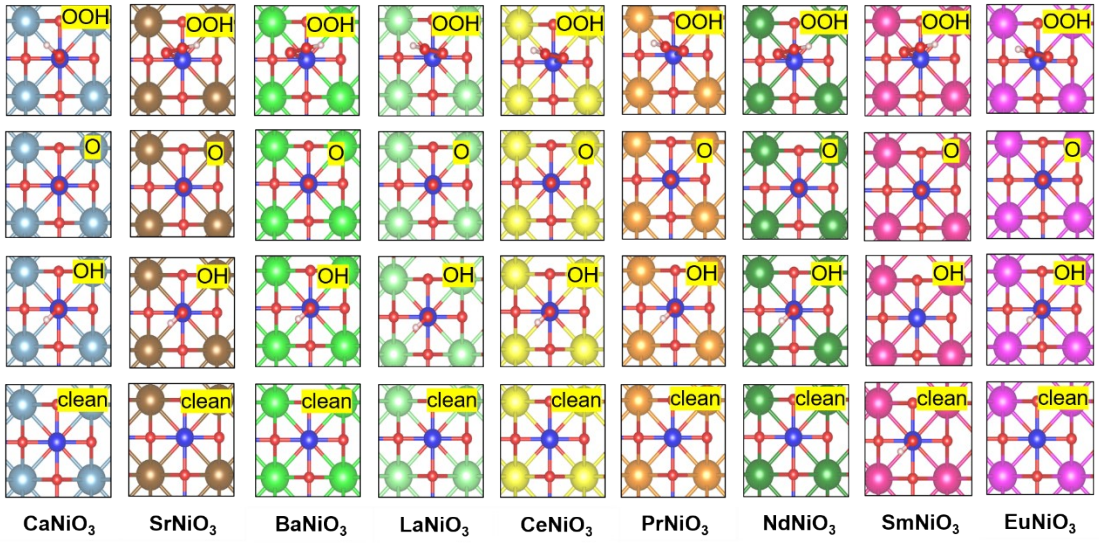

Figure S4. Adsorption models of intermediate species: *OOH, *O, and *OH of 001 Ni-O surface $ANiO_3$(A=Ca, Sr, Ba, La, Ce, Pr, Nd, Sm, Eu). Ca, Sr, Ba, La, Ce, Pr, Nd, Sm, Eu, Ni, and O atoms arepresented as light blue, brown, green, light green, yellow, orange, dark green, pink, purple, blue and red, respectively

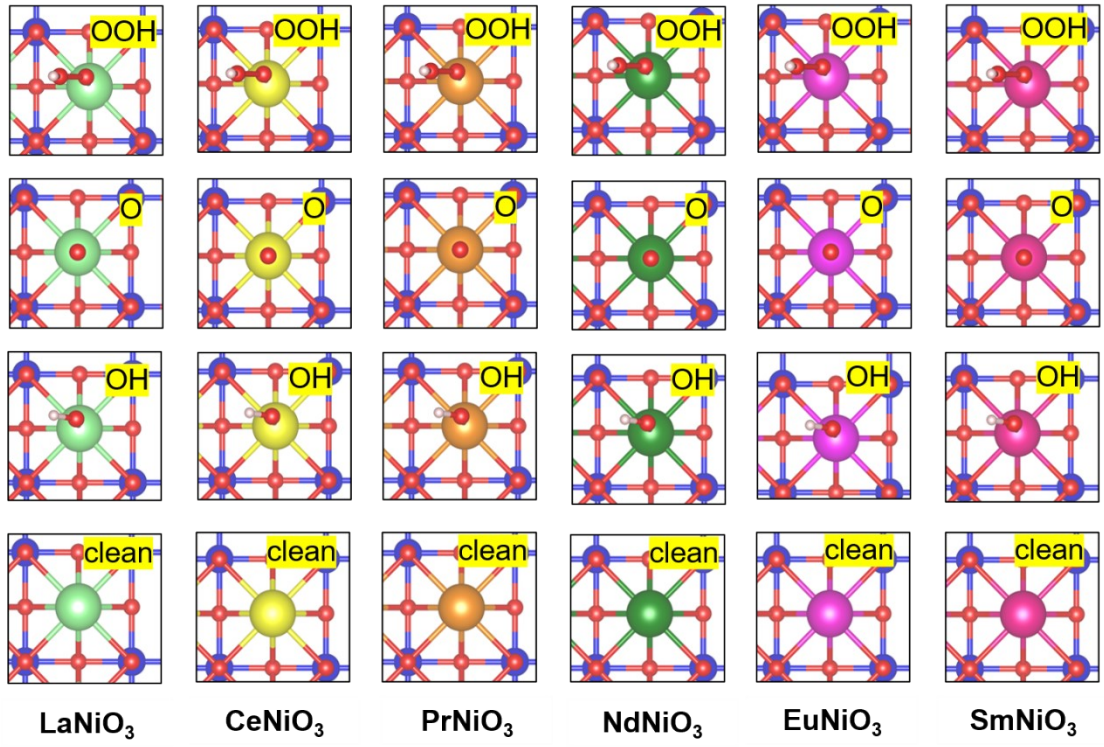

Figure S5. Adsorption models of intermediate species: *OOH, *O, and *OH of 001 AO surface $ANiO_3$(A=La, Ce, Pr, Nd, Sm, Eu). La, Ce, Pr, Nd, Sm, Eu, Ni, and O atoms arepresented as light green, yellow, orange, dark green, pink, purple, blue and red, respectively

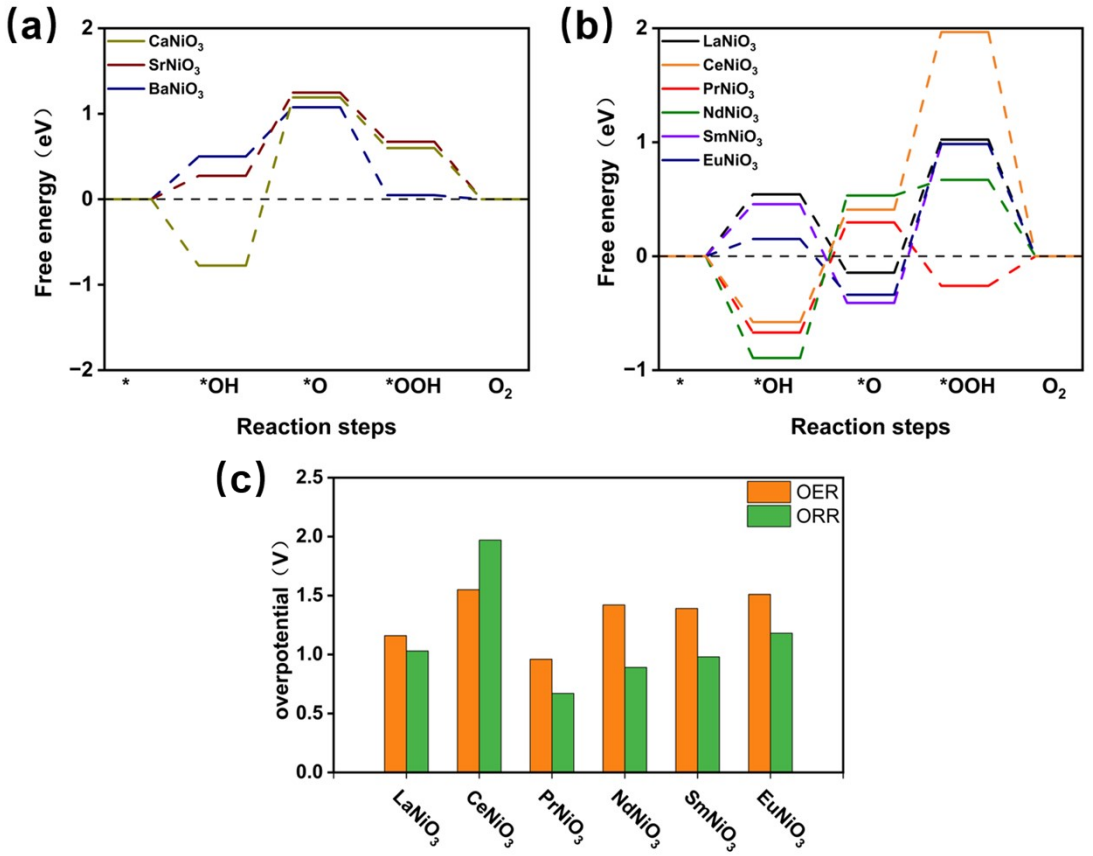

Figure S6. (a) Step diagram of alkaline earth free energy; (b) Rare earth AO surface free energy; (c) Comparison bar chart of overpotential on rare earth AO surface

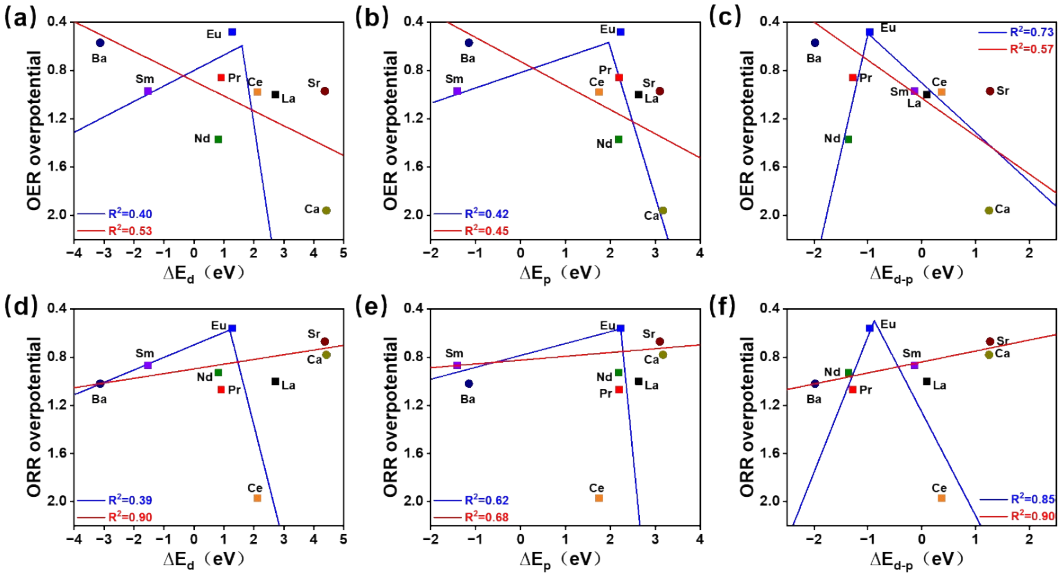

Figure S7. Structure performance relationship diagram of d-band (ΔE_d) , p-band (ΔE_p) , electron transfer energy (ΔE_{d-p}) with Ni-O surfaces OER and ORR overpotentials, respectively.

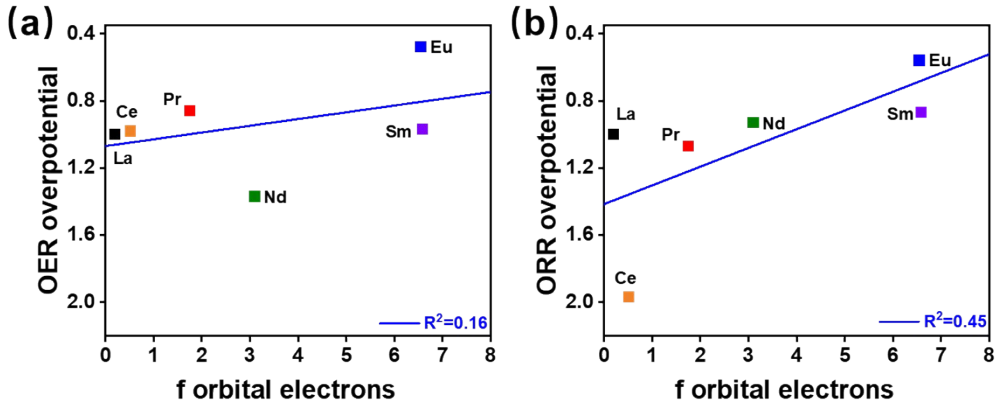

Figure S8. The relationship between the number of electrons in rare earth f-orbitals and the overpotentials of OER and ORR.

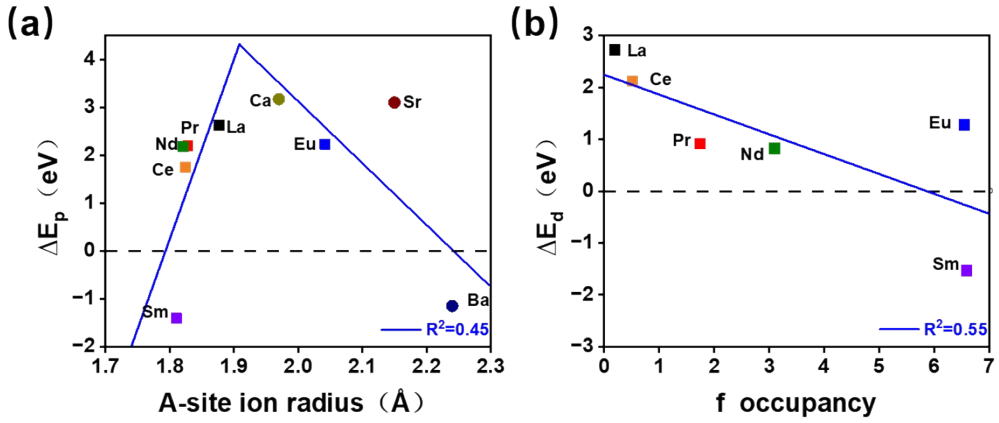

Figure S9.(a) Relationship diagram between A-site ion radius and p-band center (ΔE_p). (b) Relationship diagram between the number of electrons in rare earth f-orbitals and the center of the d-band (ΔE_d).

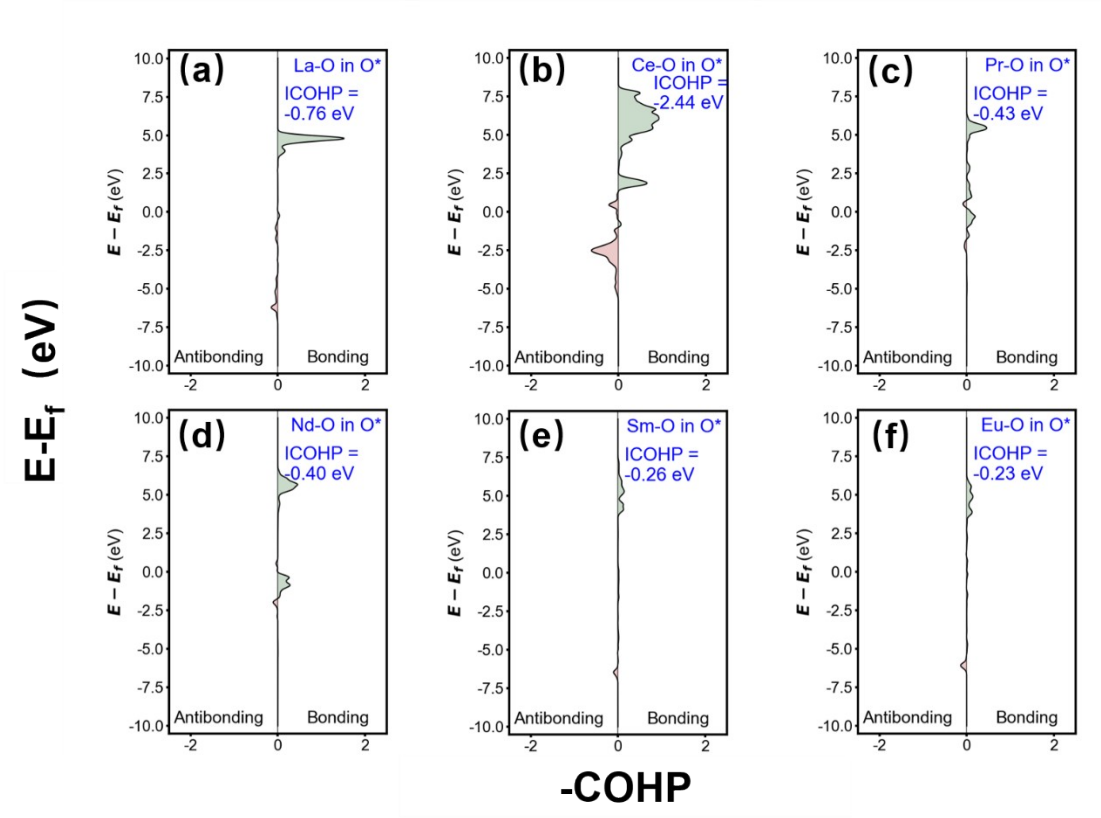

Figure S10. Cohp of A-O bond on AO surface of rare earth

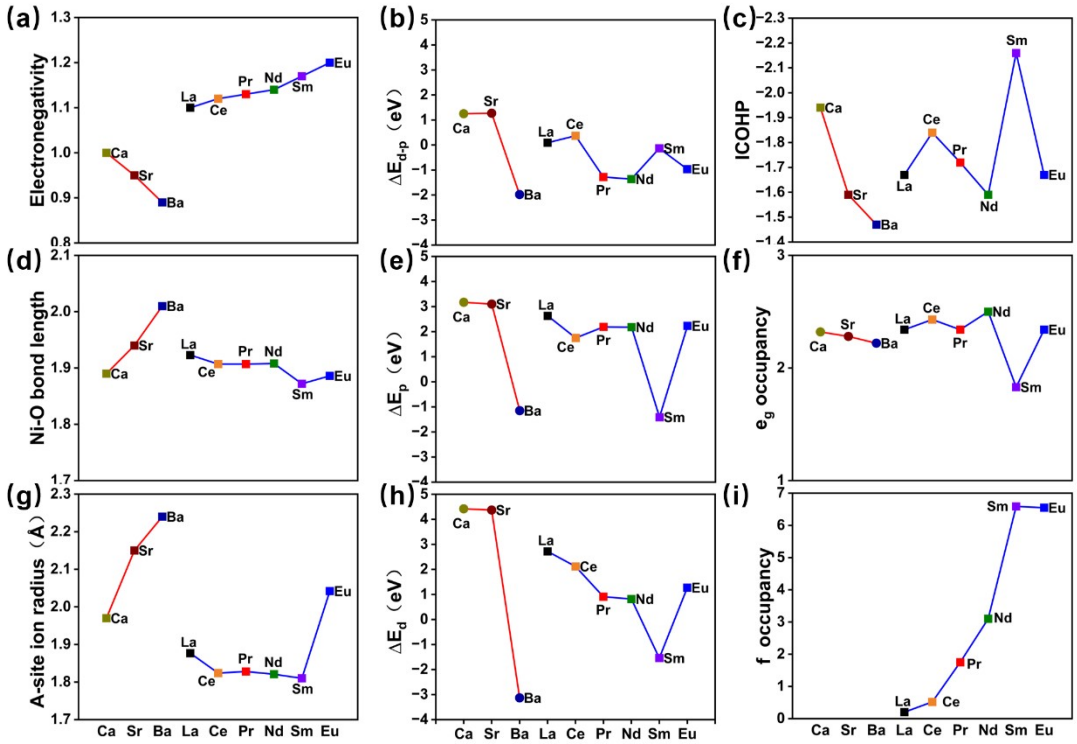

Figure S11. Overview of elemental properties and electronic structures of perovskites with different A-sites

Table S1. Detailed information on the Hubbard U values of each element in $ANiO_3$.

Elements	Pseudopotential	Valenceelectron	HubbardU
Ni	Ni	$3d^84s^2$	6.2[1]
H	H	$1s^1$	0
O	O	$2s^22p^4$	0
Ca	Ca_sv	$3s^23p^64s^2$	0
Sr	Sr_sv	$4s^24p^65s^2$	0
Ba	Ba_sv	$5s^25p^66s^2$	0
La	La	$4f^05d^16s^2$	3.7[2]
Ce	Ce	$4f^15d^16s^2$	5.0[3]
Pr	Pr	$4f^36s^2$	5.0[4]
Nd	Nd	$4f^46s^2$	4.8[5]
Sm	Sm	$4f^66s^2$	7.35[6]
Eu	Eu	$4f^76s^2$	5.0[7]

Table S2. The optimized bulk structure of E_f in each case.

Bulk	**E_f (eV/atom)**	**Space group**	**Lattice parameter (Å)**
$CaNiO_3$	-4.51	PM-3M（221）	a=b=c=3.78
$SrNiO_3$	-4.76	PM-3M（221）	a=b=c=3.88
$BaNiO_3$	-4.93	PM-3M（221）	a=b=c=4.03
$LaNiO_3$	-8.35	PM-3M（221）	a=b=c=3.84 a=b=c=3.84[8]
$CeNiO_3$	-6.49	PM-3M（221）	a=b=c=3.81
$PrNiO_3$	-6.71	PM-3M（221）	a=b=c=3.81
$NdNiO_3$	-7.95	PM-3M（221）	a=b=c=3.81
$SmNiO_3$	-7.99	PM-3M（221）	a=b=c=3.77
$EuNiO_3$	-7.61	PM-3M（221）	a=b=c=3.77

Table S3. The A parameter of $ANiO_3$ perovskite includes ion radius, Ni-O bond length, and electronegativity.

Bulk	A-site ion radius（Å）	Ni-O Bond length	Electronegativity
CaNiO3	1.970	1.890	1.00
SrNiO3	2.150	1.940	0.95
BaNiO3	2.240	2.010	0.89
LaNiO3	1.877	1.923	1.10
CeNiO3	1.824	1.907	1.12
PrNiO3	1.828	1.907	1.13
NdNiO3	1.821	1.908	1.14
SmNiO3	1.810	1.872	1.17
EuNiO3	2.042	1.886	1.20

Table S4. Calculated results of surface energy and adsorption energy (eV) of the intermediates: *OOH, *O, and *OH on $ANiO_3$∝(001) Ni-O surfaces.

Surface-BO（001）	**surface energy（J/m²）**	***OH Adsorption Energy（eV）**	***O Adsorption energy（eV）**	***OOH Adsorption energy（eV）**
$CaNiO_3$	1.21	-3.33	-2.16	-2.84
$SrNiO_3$	1.08	-2.34	-2.17	-2.75
$BaNiO_3$	0.79	-2.10	-2.32	-3.36
$LaNiO_3$	1.12	-2.04	-1.87	-2.44
$CeNiO_3$	1.01	-2.01	-1.81	-3.86
$PrNiO_3$	1.41	-1.97	-1.94	-2.36
$NdNiO_3$	1.24	-2.78	-2.21	-3.19
$SmNiO_3$	1.41	-2.18	-2.01	-2.54
$EuNiO_3$	1.99	-2.10	-2.11	-2.90

Table S5. Calculated results of surface energy and adsorption energy (eV) of the intermediates: *OOH, *O, and *OH on $ANiO_3$-(001) AO (La-Eu) surfaces.

Surface-AO（001）	**surface energy（J/m^2）**	***OH Adsorption Energy（eV）**	***O Adsorption energy（eV）**	***OOH Adsorption energy（eV）**
$LaNiO_3$	0.23	-1.93	-3.58	-2.34
$CeNiO_3$	0.14	-3.18	-3.03	-1.46
$PrNiO_3$	0.13	-3.15	-3.07	-3.62
$NdNiO_3$	0.14	-3.39	-2.83	-2.72
$SmNiO_3$	0.01	-2.05	-3.82	-2.38
$EuNiO_3$	1.51	-2.40	-3.74	-2.24

Table S6. Summarized ΔG, ZPE – TΔS, PDS, VL, max(ΔG) and ηOER for OER on all Ni-O surfaces.

		ΔG(*OH) (eV)	ΔG(*O) (eV)	ΔG(*OOH) (eV)	(ZPE – TΔS) (*OH) (eV)	(ZPE – TΔS) (*O) (eV)	(ZPE – TΔS) (*OOH) (eV)	OER PDS	OER V_L (eV)	max(ΔG) (eV)	ηOER (V)
1	$CaNiO_3$	0.45	3.19	0.64	0.26	-0.03	0.33	*OH→*O	3.19	3.19	1.96
2	$SrNiO_3$	1.50	2.20	0.65	0.32	0.02	0.31	*OH→*O	2.20	2.20	0.97
3	$BaNiO_3$	1.73	1.80	0.20	0.31	0.01	0.30	*OH→*O	1.80	1.80	0.57
4	$LaNiO_3$	1.74	2.23	0.70	0.27	-0.00	0.33	*OH→*O	2.23	2.23	1.00
5	$CeNiO_3$	1.82	2.21	-0.74	0.31	0.00	0.35	*OH→*O	2.21	2.21	0.98
6	$PrNiO_3$	1.90	2.09	0.85	0.25	0.00	0.32	*OH→*O	2.09	2.09	0.86
7	$NdNiO_3$	1.03	2.60	0.29	0.29	0.00	0.31	*OH→*O	2.60	2.60	1.37
8	$SmNiO_3$	1.63	2.20	0.73	0.29	0.00	0.31	*OH→*O	2.20	2.20	0.97
9	$EuNiO_3$	1.68	1.71	0.85	0.27	-0.01	0.35	*OH→*O	1.71	1.71	0.48

Table S7. Summarized ΔG, ZPE – TΔS, PDS, VL, max(ΔG) and ηORR for ORR on all Ni-O surfaces.

		ΔG(*OOH) (eV)	ΔG(*O) (eV)	ΔG(*OH) (eV)	(ZPE – TΔS) (*OOH) (eV)	(ZPE – TΔS) (*O) (eV)	(ZPE – TΔS) (*OH) (eV)	ORR PDS	ORR V_L (eV)	max(ΔG) (eV)	ηORR (V)
1	$CaNiO_3$	-0.63	-0.63	-3.19	0.33	-0.03	0.26	*OH→*H_2O	0.45	-0.45	0.78
2	$SrNiO_3$	-0.56	-0.65	-2.20	0.31	0.02	0.32	O_2→*OOH	0.56	-0.56	0.67
3	$BaNiO_3$	-1.18	-0.21	-1.80	0.31	0.00	0.29	*OOH→*O	0.21	-0.21	1.02
4	$LaNiO_3$	-0.23	-0.70	-2.23	0.33	-0.00	0.27	O_2→*OOH	0.23	-0.23	1.00
5	$CeNiO_3$	-1.62	0.74	-2.21	0.35	0.00	0.31	O_2→*OOH	-0.74	0.74	1.97
6	$PrNiO_3$	-0.16	-0.85	-2.09	0.32	0.00	0.25	O_2→*OOH	0.16	-0.16	1.07
7	$NdNiO_3$	-0.98	-0.29	-2.60	0.31	0.00	0.29	*OOH→*O	0.29	-0.29	0.93
8	$SmNiO_3$	-0.35	-0.73	-2.20	0.31	0.00	0.29	O_2→*OOH	0.35	-0.35	0.87
9	$EuNiO_3$	-0.66	-0.85	-1.71	0.35	-0.01	0.27	O_2→*OOH	0.66	-0.66	0.56

Table S8. Summarized ΔG, ZPE – TΔS, PDS, VL, max(ΔG) and ηOER for OER on AO(La-Eu) surfaces.

		ΔG(*OH) (eV)	ΔG(*O) (eV)	ΔG(*OOH) (eV)	(ZPE – TΔS) (*OH) (eV)	(ZPE – TΔS) (*O) (eV)	(ZPE – TΔS) (*OOH) (eV)	OER PDS	OER V_L (eV)	max(ΔG) (eV)	ηOER (V)
1	$LaNiO_3$	1.63	0.82	2.39	0.18	-0.04	0.26	*OH→*O	2.39	2.39	1.16
2	$CeNiO_3$	0.65	2.21	2.78	0.31	0.04	0.32	*OH→*O	2.78	2.78	1.55
3	$PrNiO_3$	0.55	2.19	0.67	0.18	-0.02	0.25	*OH→*O	2.19	2.19	0.96
4	$NdNiO_3$	0.33	2.65	1.36	0.21	-0.02	0.28	*OH→*O	2.65	2.65	1.42
5	$SmNiO_3$	1.68	0.36	2.62	0.22	0.02	0.25	*O→*OOH	2.62	2.62	1.39
6	$EuNiO_3$	1.38	0.74	2.74	0.26	0.01	0.30	*O→*OOH	2.74	2.74	1.51

Table S9. Summarized ΔG, ZPE – TΔS, PDS, VL, max(ΔG) and ηORR for ORR on AO(La-Eu) surfaces.

		ΔG(*OOH) (eV)	ΔG(*O) (eV)	ΔG(*OH) (eV)	(ZPE – TΔS) (*OOH) (eV)	(ZPE – TΔS) (*O) (eV)	(ZPE – TΔS) (*OH) (eV)	ORR PDS	ORR V_L (eV)	max(ΔG) (eV)	ηORR (V)
1	$LaNiO_3$	-0.20	-2.39	-0.54	0.26	-0.04	0.18	O_2→*OOH	0.20	-0.20	1.03
2	$CeNiO_3$	0.73	-2.78	-2.21	0.32	0.04	0.31	O_2→*OOH	-0.73	0.73	1.97
3	$PrNiO_3$	-1.48	-0.67	-2.19	0.25	-0.02	0.18	O_2→*OOH	0.56	-0.56	0.67
4	$NdNiO_3$	-0.56	-1.36	-2.65	0.28	-0.02	0.21	*OOH→*O	0.33	-0.33	0.89
5	$SmNiO_3$	-0.24	-2.62	-0.36	0.25	0.02	0.22	O_2→*OOH	0.24	-0.24	0.98
6	$EuNiO_3$	-0.05	-2.74	-0.74	0.30	0.01	0.26	O_2→*OOH	0.05	-0.05	1.18

Table S10. Comparison of band gap data for $ANiO_3$ perovskite.

Bulk	Theoretical bandgap calculation	Material project bandgap	Experimental
$CaNiO_3$	0.00eV	/	/
$SrNiO_3$	0.00eV	0.00eV	/
$BaNiO_3$	0.00eV	0.00eV	/
$LaNiO_3$	0.00eV	0.00eV	0.00eV[9]
$CeNiO_3$	0.00eV	0.00eV	/
$PrNiO_3$	0.00eV	/	/
$NdNiO_3$	0.00eV	/	/
$SmNiO_3$	0.00eV	0.00eV	/
$EuNiO_3$	0.00eV	0.00eV	/

Table S11. Electronic structure descriptors of $ANiO_3$ perovskite (d-band center, p-band center, electron transfer energy （ΔE_{d-p}） , e_g orbital occupancy and f orbital electrons)

Bulk	d-band center	p-band center	e_g orbital occupancy	Electron transfer energy（ΔE_{d-p}）	f orbital electrons
CaNiO3	4.42	3.17	2.34	1.25	/
SrNiO3	4.37	3.10	2.43	1.27	/
BaNiO3	-3.13	-1.15	2.34	-1.98	/
LaNiO3	2.72	2.63	2.34	0.09	0.20
CeNiO3	2.12	1.75	2.43	0.37	0.52
PrNiO3	0.91	2.19	2.34	-1.28	1.75
NdNiO3	0.82	2.18	2.50	-1.36	3.10
SmNiO3	-1.54	-1.41	1.83	-0.13	6.59
EuNiO3	1.27	2.23	2.34	-0.96	6.55

Table S12. Bader charge analysis (in |e|) of Ni-active site on $ANiO_3$ perovskite oxides during ORR and OER.

Number	Catalysts	$\Delta\delta_B$ (clean)	$\Delta\delta_B$ (*OH)	$\Delta\delta_B$ (*O)	$\Delta\delta_B$ (*OOH)	$\Delta\delta_{surface}$ (*OH)	$\Delta\delta_{*OH}$ (*OH)	$\Delta\delta_{surface}$ (*O)	$\Delta\delta_{*O}$ (*O)	$\Delta\delta_{surface}$ (*OOH)	$\Delta\delta_{*OOH}$ (*OOH)
1	$CaNiO_3$	+1.38	+1.13	+1.38	+0.83	+0.68	-0.68	+0.36	-0.36	+0.27	-0.27
2	$SrNiO_3$	+1.35	+1.08	+1.39	+1.04	+0.66	-0.66	+0.34	+0.34	+0.21	-0.21
3	$BaNiO_3$	+1.29	+1.32	+1.38	+1.25	+0.77	-0.77	+0.31	-0.31	+0.30	-0.30
4	$LaNiO_3$	+1.30	+1.40	+1.41	+1.36	+0.84	-0.84	+0.38	-0.38	+0.30	-0.30
5	$CeNiO_3$	+1.23	+1.10	+1.21	+0.92	+0.84	-0.84	+0.21	-0.21	+0.13	-0.13
6	$PrNiO_3$	+1.32	+1.04	+1.43	+1.37	+0.80	-0.80	+0.37	-0.37	+0.36	-0.36
7	$NdNiO_3$	+1.34	+1.35	+1.32	+1.17	+0.90	-0.90	+0.31	-0.31	+0.35	-0.35
8	$SmNiO_3$	+1.26	+1.30	+1.32	+1.29	+0.88	-0.88	+0.34	-0.34	+0.30	-0.30
9	$EuNiO_3$	+1.43	+1.23	+1.31	+1.13	+0.87	-0.87	+0.33	-0.33	+0.26	-0.26

Table S13. Bader charge analysis (in |e|) of B atoms on $ANiO_3$ perovskite oxides.

Catalysts	$\Delta_{\delta avg}$ (B-site)	$\Delta_{\delta avg}$ (O-site)
$CaNiO_3$	+1.38	-0.96
$SrNiO_3$	+1.35	-0.97
$BaNiO_3$	+1.29	-0.94
$LaNiO_3$	+1.30	-1.09
$CeNiO_3$	+1.23	-1.10
$PrNiO_3$	+1.32	-1.11
$NdNiO_3$	+1.34	-1.11
$SmNiO_3$	+1.26	-1.08
$EuNiO_3$	+1.43	-0.95

Table S14. Element properties - electronic structure descriptor correspondence table

	Element properties		Electronic structure descriptor			
Catalysts	A-site ion radius	electronegativity	ΔE_d	ΔE_p	ΔE_{d-p}	e_g
$CaNiO_3$	1.970	1.00	4.42	3.17	1.25	2.34
$SrNiO_3$	2.150	0.95	4.37	3.10	1.27	2.43
$BaNiO_3$	2.240	0.89	-3.13	-1.15	-1.98	2.34
$LaNiO_3$	1.877	1.10	2.72	2.63	0.09	2.34
$CeNiO_3$	1.824	1.12	2.12	1.75	0.37	2.43
$PrNiO_3$	1.828	1.13	0.91	2.19	-1.28	2.34
$NdNiO_3$	1.821	1.14	0.82	2.18	-1.36	2.50
$SmNiO_3$	1.810	1.17	-1.54	-1.41	-0.13	1.83
$EuNiO_3$	2.042	1.20	1.27	2.23	-0.96	2.34

Table S15 Summarized ICOHP values of Ni–O and A–O/Ni–O bonds for all $ANiO_3$ perovskites

Catalysts	ICOHP of Ni–O (BO-terminated) / eV	ICOHP of A–O (AO-terminated) / eV
$CaNiO_3$	-1.94	/
$SrNiO_3$	-1.59	/
$BaNiO_3$	-1.47	/
$LaNiO_3$	-1.67	-0.76
$CeNiO_3$	-1.84	-2.44
$PrNiO_3$	-1.72	-0.43
$NdNiO_3$	-1.59	-0.40
$SmNiO_3$	-2.16	-0.26
$EuNiO_3$	-1.67	-0.23

Table S16 Radar chart data sheet

	Rare earth OER overpotential	Rare earth ORR overpotential	Alkaline earth OER overpotential	Alkaline earth ORR overpotential
d-band center	0.40	0.39	0.53	0.90
p-band center	0.42	0.62	0.45	0.68
ICOHP	0.48	0.85	0.74	0.20
e_g	0.71	0.84	0.87	0.56
ΔE_{d-p}	0.85	0.73	0.90	0.57
electronegativity	0.31	0.36	0.91	0.50
A-site ion radius	0.61	0.27	0.99	0.26
Ni-O Bond length	0.59	0.38	0.89	0.54
F orbital electrons	0.13	0.45	/	/

Table S17 Normalized tabular data for optimal descriptor of radar graph

$new\_value = (value - min)/(max - min)$

	d-band center	e_g	ΔE_{d-p}	A-site ion radius
$CaNiO_3$	1.00	1.00	0.99	0.00
$SrNiO_3$	0.99	0.60	1.00	0.67
$BaNiO_3$	0.00	0.00	0.00	1.00

	ICOHP	e_g	ΔE_{d-p}	A-site ion radius
$LaNiO_3$	0.86	0.76	0.84	0.29
$CeNiO_3$	0.56	0.90	1.00	0.06
$PrNiO_3$	0.77	0.76	0.05	0.08
$NdNiO_3$	1.00	1.00	0.00	0.05
$SmNiO_3$	0.00	0.00	0.71	0.00
$EuNiO_3$	0.86	0.76	0.23	1.00

Table S18 Univariate linear regression results of OER/ORR activity and key descriptors of alkaline earth system

Activity type	Descriptor name	Fitting equation	Coefficient of determination	P value
OER	e_g	ηOER= 1.33* （e_g） +0.33	0.88	0.22
OER	A-site ion radius	ηOER= -1.40* （A-site ion radius） +1.95	0.99	0.03
ORR	ΔE_{d-p}	ηORR= -0.29* （ΔE_{d-p}） +1.02	0.91	0.19
ORR	d-band center	ηORR= -0.29* （d-band center） +1.01	0.90	0.20

Table S19 Multiple linear regression results of OER activity and key descriptors of rare earth system

Descriptor name	Denormalization coefficient (η : V; descriptor: normalized value)	Standardization coefficient (beta, weight)	P value	Correlation direction
ICOHP	0.61	0.76	0.70	positive correlation
e_g	-0.26	-0.32	0.84	negative correlation
ΔE_{d-p}	0.05	0.07	0.91	positive correlation
A-site ion radius	-0.74	-0.98	0.32	negative correlation

Note: the regression is based on the normalized DFT data of six rare earth systems; Overall model indicators: multiple R=0.8824, R^2 =0.7786, significance F=0.6537 (due to the limited number of data points, focus on the weight trend of standardization coefficient); The greater the absolute value of the standardization coefficient (beta), the higher the weight of the descriptor on OER activity.

Table S20 Multiple linear regression results of ORR activity and key descriptors of rare earth system

Descriptor name	Denormalization coefficient (η : V; descriptor: normalized value)	Standardization coefficient (beta, weight)	P value	Correlation direction
ICOHP	-1.83	-1.37	0.23	negative correlation
e_g	2.22	1.64	0.17	positive correlation
ΔE_{d-p}	0.34	0.31	0.39	positive correlation
A-site ion radius	-0.29	-0.23	0.45	negative correlation

Note: the regression is based on the normalized DFT data of six rare earth systems; Overall model indicators: multiple R=0.9859, R^2 =0.9720, significance F=0.2486 (due to the limited number of data points, focus on the weight trend of standardization coefficient); The greater the absolute value of the standardization coefficient (beta), the higher the weight of the descriptor on ORR activity.

References

[1] J.M. Munro, K. Latimer, M.K. Horton, et al., An improved symmetry-based approach to reciprocal space path selection in band structure calculations, npj Comput. Mater. 6(1) (2020).
[2] S. Somdee, M. Rittiruam, T. Saelee, et al., First-principles investigations on effects of B-site substitution (B═Mn, Fe, and Co) on La-based perovskite oxides as bifunctional electrocatalysts for rechargeable metal–air batteries, Advanced Theory and Simulations 7(6) (2024) 2301235.
[3] X. Wang, M. Li, Z. Wu, In situ spectroscopic insights into the redox and acid-base properties of ceria catalysts, Chinese Journal of Catalysis 42(12) (2021) 2122-2140.
[4] M.B. Kanoun, A.H. Reshak, N. Kanoun-Bouayed, et al., Evidence of Coulomb correction and spin–orbit coupling in rare-earth dioxides CeO_2, PrO_2 and TbO_2: An ab initio study, J. Magn. Magn. Mater. 324(7) (2012) 1397-1405.
[5] Q. Wu, G. Liu, H. Shi, et al., Impact of Nd doping on electronic, optical, and magnetic properties of ZnO: A GGA + U study, Molecules, 2023, p. 7416.
[6] J. Feng, B. Xiao, C.L. Wan, et al., Electronic structure, mechanical properties and thermal conductivity of $Ln_2Zr_2O_7$ (Ln=La, Pr, Nd, Sm, Eu and Gd) pyrochlore, Acta Mater. 59(4) (2011) 1742-1760.
[7] Z.-Y. Zhao, W.-W. Dai, Structural, electronic, and optical properties of Eu-doped BiO_X (X = F, Cl, Br, I): A DFT+U Study, Inorg. Chem. 53(24) (2014) 13001-13011.
[8] Z. Wu, M. Fan, H. Jiang, et al., Harnessing the Unconventional Cubic Phase in 2D $LaNiO_3$ Perovskite for Highly Efficient Urea Oxidation, Angew. Chem. Int. Ed. 64(1) (2025) e202413932.
[9] L. Wang, K.A. Stoerzinger, L. Chang, et al., Tuning bifunctional oxygen electrocatalysts by changing the A-site rare-earth element in perovskite nickelates, Adv. Funct. Mater. 28(39) (2018) 1803712.